Materials Advances

ROYAL SOCIETY OF CHEMISTRY

PAPER

View Article Online
View Journal | View Issue

Check for updates

Cite this: *Mater. Adv.*, 2022, 3, 7618

'Template-free' synthesis of self-assembled micro-spikes resulting in 'sea-urchin'-like carbon structures for suppressing electromagnetic radiation†

Vidyashree M. P.,[a] Kumari Sushmita,[bc] Kokila M. K.*[a] and Suryasarathi Bose*[b]

We report the facile 'template-free' synthesis of self-assembled 'micro-spikes', resulting in sea-urchin-like carbon structures that can suppress incoming electromagnetic (EM) radiation, which may not be achievable with conventional flake-type dispersed composites. Herein, we synthesized 'carbon-urchins' (C-urchins) from the self-assembly of short carbon fibers (CFs) *via* a facile one-pot synthesis method and then incorporated them into an epoxy matrix to obtain high-performance EMI shielding materials. To gain mechanistic insight, the C-urchins were doped with different dopants, such as magnetic nano-Fe_3O_4 (C-F urchins), conducting nano-Ag particles (C-A urchins), and dielectric nano-SiO_2 (C-S urchins), to evaluate the influence of the dopant on the EMI shielding performance. Interestingly, all three doped C-urchin types in an epoxy matrix showed excellent absorption-dominated shielding (>99%) in the K-band region, with shielding effectiveness (SE_T) of up to −32 dB. The spatial distribution of the C-urchins was controlled in the epoxy composites to achieve the highest SE_T values for the prepared composites. The thermal properties of the composites were similar to those of neat epoxy; however, the storage modulus was enhanced in the composites. To this end, while high loading of conducting filler is required to meet commercial standards, resulting in processing difficulties, C-urchin-filled composites can open up new avenues in this field. The micro-spikes of the C-urchins can scatter/absorb incoming EM radiation through coupling with the fields.

Received 20th June 2022,
Accepted 23rd July 2022

DOI: 10.1039/d2ma00715k

rsc.li/materials-advances

Open Access Article. Published on 02 August 2022. Downloaded on 2/10/2026 5:06:23 AM.
This article is licensed under a Creative Commons Attribution-NonCommercial 3.0 Unported Licence.

Introduction

Over the years, the rapid development and large-scale usage of advanced electronic devices, wireless communications, instruments in military and civil areas, *etc.*, have made human life more convenient and comfortable. This huge dependence on electronic equipment has created a serious environmental problem in the form of electromagnetic interference (EMI).[1,2] EMI refers to the interference of the electromagnetic signals from one electronic device with those of another device by means of radiated paths, conducted paths, or both.[3] As a result, these unwanted electromagnetic signals may adversely affect the performance of nearby devices.[4] EMI not only produces noise in signals, but it may also affect human health. Therefore, to minimize the impact of EMI, active research is ongoing to develop efficient EMI shielding materials capable of blocking EM radiation over a broad frequency range.[1]

An EM wave consists of electric and magnetic components perpendicular to each other. The direction of the propagation of the EM wave is perpendicular to both the electric and magnetic components.[5,6] EMI shielding takes place due to three phenomena: the reflection of the EM waves at the interface due to impedance mismatch; the absorption of EM waves within the shielding material due to conduction, dielectric and magnetic loss; and the multiple reflections of the EM wave within the shield at filler-polymer interfaces.[7,8] Hence the total shielding effectiveness (SE_T) is contributed to by either one or a combination of these phenomena.[9]

Conventionally, metals and metallic composites have been used extensively as EMI shielding materials because of their high conductivity, which makes them good reflectors due to the availability of a large number of free electrons.[10,11] The main drawback of using metals as shielding materials is that the electric field inside the metal is zero; therefore, the incoming EM waves are reflected/scattered back into the environment, which can further disturb the functioning of nearby devices.

[a] *Department of Physics, Bangalore University, Bangalore-560056, Karnataka, India. E-mail: drmkkokila@gmail.com*
[b] *Department of Materials Engineering, Indian Institute of Science Bangalore-560012, Karnataka, India. E-mail: sbose@iisc.ac.in*
[c] *Centre for Nano Science and Engineering, Indian Institute of Science, Bengaluru-560012, India*

† Electronic supplementary information (ESI) available. See DOI: https://doi.org/10.1039/d2ma00715k

© 2022 The Author(s). Published by the Royal Society of Chemistry

Open Access Article. Published on 02 August 2022. Downloaded on 2/10/2026 5:06:23 AM.
This article is licensed under a Creative Commons Attribution-NonCommercial 3.0 Unported Licence.

Apart from this, metals suffer from several other issues, like having a high density, being prone to corrosion, having poor chemical resistance, and creating processing difficulties. Even though metals allow excellent shielding, they are not very attractive when it comes to electronic devices, which are becoming thinner and lighter day by day.[3,12] On the other hand, polymers rightly fit in this space owing to their light weight and ease of integration into existing processes, making them a potential candidate for designing composites with multifunctional properties. Epoxy is one of the most important classes of thermoset polymers, which are widely used for structural and high-performance applications due to their unique combination of thermal, mechanical, and electrical properties.[13,14] Epoxy offers very high strength, superior adhesion to various substrates, corrosion resistance, chemical resistance, effective insulation in electronic devices, and good wetting properties, making it well suited for several applications.[14] Hence these impressive characteristics of epoxy make it an ideal candidate for use in the composite industry.[15–19] However, due to their insulating nature and lack of electric and magnetic dipoles, most polymers are transparent to EM waves. Epoxy is one such insulative polymer, and it exhibits SE_T of 0 dB. However, as already mentioned, epoxy has found several applications in the electronics and aerospace sectors, where EMI shielding is also required. Therefore, there is a need to incorporate certain magnetic/conducting/dielectric fillers to improve the EMI shielding properties of epoxy-based composites.[20,21]

To incorporate magnetic/conducting/dielectric fillers, researchers have opted for hybrid approaches or architectural tweaking. A single monolith with nano-flakes dispersed in a matrix is not amenable to meeting the stringent requirements; hence, research has focused on designing hybrid, core-shell, and multilayered structures.[7,10,22,23] However, such strategies involve cumbersome synthesis procedures and too many parameters that require precise control. Among the various fillers that have been researched, carbon-based nanofillers, such as carbon nanotubes (CNTs), graphene, and carbon fibers (CFs), have attracted a great deal of attention for designing efficient shielding materials and effectively reinforcing composites.[8,24–27] In carbonaceous derivatives, CFs have shown enormous potential for designing composites/laminates with key attributes like light weight, high tensile strength, high modulus values, low thermal expansion coefficients, and exceptional durability.[19,28–30] In addition, carbon fibers also show excellent electrical and thermal properties, and they can be used for various applications depending on the requirements. Also, carbon fibers act as a waveguide and result in excellent shielding effectiveness in laminates/composites.[31]

To further enhance the shielding abilities of composites, metallic, magnetic, and dielectric nanoparticles are largely used. These fillers include Ag, Cu, Fe_3O_4, SiO_2, ZnO, Fe, and their alloys. With the addition of dielectric and magnetic fillers, the absorption percentage during shielding can be enhanced.[32–34] Epoxy/CF composites with CF modification have been extensively studied by researchers in the last decade. Gholampoor *et al.*[35] prepared nano-Fe_3O_4 powder *via* a co-precipitation method and deposited this on CFs using an electrophoretic deposition (EPD) method; it was then incorporated into epoxy. They observed that the SE_T value for a 2 mm-thick sample was −23 dB in the range of 8.2–12.4 GHz for 20 wt% nano-Fe_3O_4/CF. Cheng *et al.*[36] prepared Ag/CF/polyaniline (PANI) composites, with PANI particles wrapping the silver-plated CFs, *via* in-situ polymerization, and these were incorporated in epoxy. Here, Ag/CF was prepared *via* an electroless plating method. They observed that the epoxy composite with Ag/CF/PANI had homogenously dispersed filler and exhibited an SE_T value of −8 dB at 4.5 wt% loading for a 2 mm sample. Movassagh-Alanagh *et al.*[37] introduced multi-walled carbon nanotubes and Fe_3O_4 nanoparticles onto CFs through an electrophoretic co-deposition process. Fe_3O_4/multiwall carbon nanotubes@CF was incorporated as a filler into epoxy resin. The sample exhibited an SE_T value of −35 dB with a thickness of 5 mm in the range of 8.2–18 GHz. There is limited literature on SiO_2-decorated CFs for EMI shielding applications, but SiO_2 has been extensively used for EMI shielding applications due to its dielectric loss properties.[38–40] The primary objective of this work is to enhance the absorption-based EMI shielding performance of epoxy composites. Hence, as mentioned above, there should be a synergetic effect between the conducting, magnetic, and dielectric components. These materials will lead to better impedance matching on the surface, thus resulting in the reduction of the overall EM reflection.[41,42]

In light of this discussion, herein, we have designed light-weight epoxy-based composites with high absorption-based EMI shielding performance using sea-urchin-like carbon structures (C-urchins) derived from the self-assembly of short carbon fibers following the refluxing of the fibers under acidic conditions. To gain mechanistic insight, C-urchins were doped with magnetic nanoparticles (here Fe_3O_4), conducting nanoparticles (here Ag), or dielectric nanoparticles (here SiO_2) to understand the role of dopants in influencing the EMI shielding performance in the composites. Dispersing carbon fibers is challenging in an epoxy matrix, as the viscosity beyond a certain concentration increases greatly, creating processing challenges. However, our strategy demonstrates that self-assembling carbon fibers to yield C-urchins is easy in terms of handling, and the spatial dispersion can be well controlled to tune the properties of the composite. The synthesis protocol adopted here is industrially scalable and can help guide researchers working in this area in both academia and industry.

Experimental section

Materials

Epoxy resin (bisphenol-*F*-epichlorohydrin, EPOLAM 8052) and an amine-based hardener (2,2′-dimethyl-4,4′methylene bis (cyclohexylamine)) were provided by Axson technologies (France). Short CFs with a length of 6 mm and diameter of about 7 μm were commercially obtained from SGL carbon

Open Access Article. Published on 02 August 2022. Downloaded on 2/10/2026 5:06:23 AM. This article is licensed under a Creative Commons Attribution-NonCommercial 3.0 Unported Licence.

company. Ferric chloride hexahydrate ($FeCl_3 \cdot 6H_2O$; LR 98%) was obtained from Thomas Baker. Ethanol, hydrazine hydrate ($H_4N_2 \cdot H_2O$; 99%), ethylene glycol ($C_2H_6O_2$), urea (NH_2CONH_2), silver nitrate, liquid ammonia, and tetraethyl orthosilicate were procured from SDFCL.

Synthesis of C-urchins

500 mg of pristine CFs was taken and added to acid solution (40 ml of distilled water and 360 ml of HNO_3). The solution was bath-sonicated for 30 min and kept under stirring for 24 h at 80 °C in an oil bath. The resultant solution was filtered, washed repeatedly with distilled water, and kept in an oven at 80 °C for drying. The yield of C-urchins obtained is 99%. The preparation procedure of C-urchins is shown in Fig. 1.

Preparation of C-F urchins. To decorate Fe_3O_4 particles onto C-urchins, typically, 50 mg of C-urchins was dispersed in 40 ml of ethylene glycol and stirred for 15 min. Later, the resultant dispersion was added to a solution containing $FeCl_3 \cdot 6H_2O$, which was prepared *via* dissolving 100 mg of $FeCl_3 \cdot 6H_2O$ and 250 mg of urea in 10 ml of ethylene glycol. Thereafter, 1 ml of hydrazine hydrate was added to the resultant dispersion. The dispersion was stirred well again for 5 min. The obtained dispersion was immediately transferred into a Teflon-lined stainless steel autoclave and kept in a preheated oven at 200 °C for 10 h.[43] After the completion of the reaction, the autoclave was allowed to cool down to room temperature. Finally, the resultant precipitate was collected, washed with distilled water and ethanol, and dried for further use. It was observed that the C-F urchins were magnetic, as shown in Fig. 1. The synthesis procedure for C-F urchins is shown in Fig. 1(a).

Preparation of C-A urchins. To decorate Ag particles onto C-urchins, 50 mg of C-urchins was added to 50 ml of distilled water along with the addition of 0.01 M $AgNO_3$. The dispersion was stirred for 30 min, and then 100 μl of hydrazine hydrate was added to it. Later, the entire dispersion was transferred to a round-bottom flask, and this was refluxed at 90 °C for 24 h. Once the reaction was completed, *i.e.*, after 24 h, the dispersion was centrifuged, washed several times with distilled water, and dried to obtain C-A urchins.[44] A diagram illustrating the synthesis procedure is shown in Fig. 1(b).

Preparation of C-S urchins. To decorate SiO_2 particles onto C-urchins, 50 mg of C-urchins was added to 50 ml of ethanol and this was stirred for 30 min. Later, 0.5 ml of TEOS and 2 ml of aqueous ammonia was added, and this was kept under stirring for about 6 h at room temperature. Once the reaction was completed, the dispersion was centrifuged with ethanol and dried for further use.[45] A diagram illustrating the synthesis procedure is shown in Fig. 1(c).

Preparation of epoxy composites containing different doped C-urchins. Neat epoxy and epoxy composites containing C-urchins, C-F urchins, C-A urchins, and C-S urchins were prepared. Initially, epoxy and hardener (at a weight ratio of 100 : 37) were kept mixing for 15 min. For the adequate dispersion of filler in the polymer matrix, mechanical mixing was performed using an overhead stirrer (Heidolph RZR 2102) at 500 rpm. The mixture was kept under vacuum to remove air bubbles. Once the bubbles were removed, epoxy composites were prepared *via* varying the spatial distribution of fillers (*i.e.*, different types of C urchins). Then, the mixture of epoxy and hardener (prepared in the previous step) was carefully poured into a Teflon-coated aluminum mold. A bed of urchins was arranged manually in the mold first with no overlap, as is shown in Fig. 2. The mold was then kept in the oven for curing and post-curing. It was pre-cured at 60, 80, and 100 °C for 1 h each, followed by post-curing at 120 °C for 2 h.[46] The sample codes for easy representation are as follows: C-urchins close (which means closely packed), C-urchins far (loosely packed), C-F urchins (closely packed), C-A urchins (closely packed), and C-S urchins (closely packed). Rectangular samples were fabricated for dynamic mechanical analysis (DMA) and EMI shielding and electrical conductivity measurements.

Characterization

The doping of magnetic, conducting, or dielectric particles onto C-urchins was confirmed *via* scanning electron microscopy and X-ray diffraction. XRD analysis was performed using XPERT Pro apparatus from PANalytical in the 2θ range of 5–80°, using a CuKα radiation source (λ = 1.5406 Å, 40 kV, and 30 mA). The carboxylic functionalization of C-urchins was confirmed *via* Fourier-transform infrared (FTIR) spectroscopy using a PerkinElmer GX spectrometer in the range of 4000–400 cm^{-1}. The decoration of Fe_3O_4, Ag, and SiO_2 onto CFs was assessed using field-emission scanning electron microscopy (FESEM, model-ULTRA 55, bought from Carl Zeiss). Energy dispersive X-ray spectroscopy (EDS) analysis was carried out to obtain a rough estimate of the percentage of filler on the C-urchins. Thermal degradation studies of epoxy composites were performed using a thermogravimetric analyzer (TGA, model-Q500, bought from TA instruments) in the temperature range of 30–900 °C in a nitrogen environment. Dynamic mechanical thermal analysis was done using a three-point bending clamp on a TA Q800 dynamic mechanical analyzer (DMA) in the temperature range of 35–200 °C at a constant vibrating frequency of 1 Hz and with an amplitude of 15 μm. The AC electrical conductivity was measured (specimen dimensions: diameter, 10 mm; thickness, 1 mm) using an impedance analyzer (Alpha-A analyzer bought from Novocontrol, Germany) over a broad frequency range of 10^{-1} to 10^7 Hz at room temperature. Limiting oxygen index (LOI) tests were carried out according to ASTM D2863 standards using apparatus bought from Concept Equipment Ltd, UK. For LOI testing, first the sample was mounted on a holder, followed by ignition using a burner, and then measurements were recorded. For heat dissipation measurements, the sample was heated with a laser with a wavelength of 808 nm for 50 s and then the laser was switched off and the sample was allowed to cool for 50 s. IR imaging was done using an IR camera (brought from FLUKE). EMI shielding measurements were carried out using a Keysight (model: Fieldfox microwave analyzer N9918A) vector network analyzer (VNA) in a broadband frequency

 © 2022 The Author(s). Published by the Royal Society of Chemistry

Open Access Article. Published on 02 August 2022. Downloaded on 2/10/2026 5:06:23 AM.
This article is licensed under a Creative Commons Attribution-NonCommercial 3.0 Unported Licence.

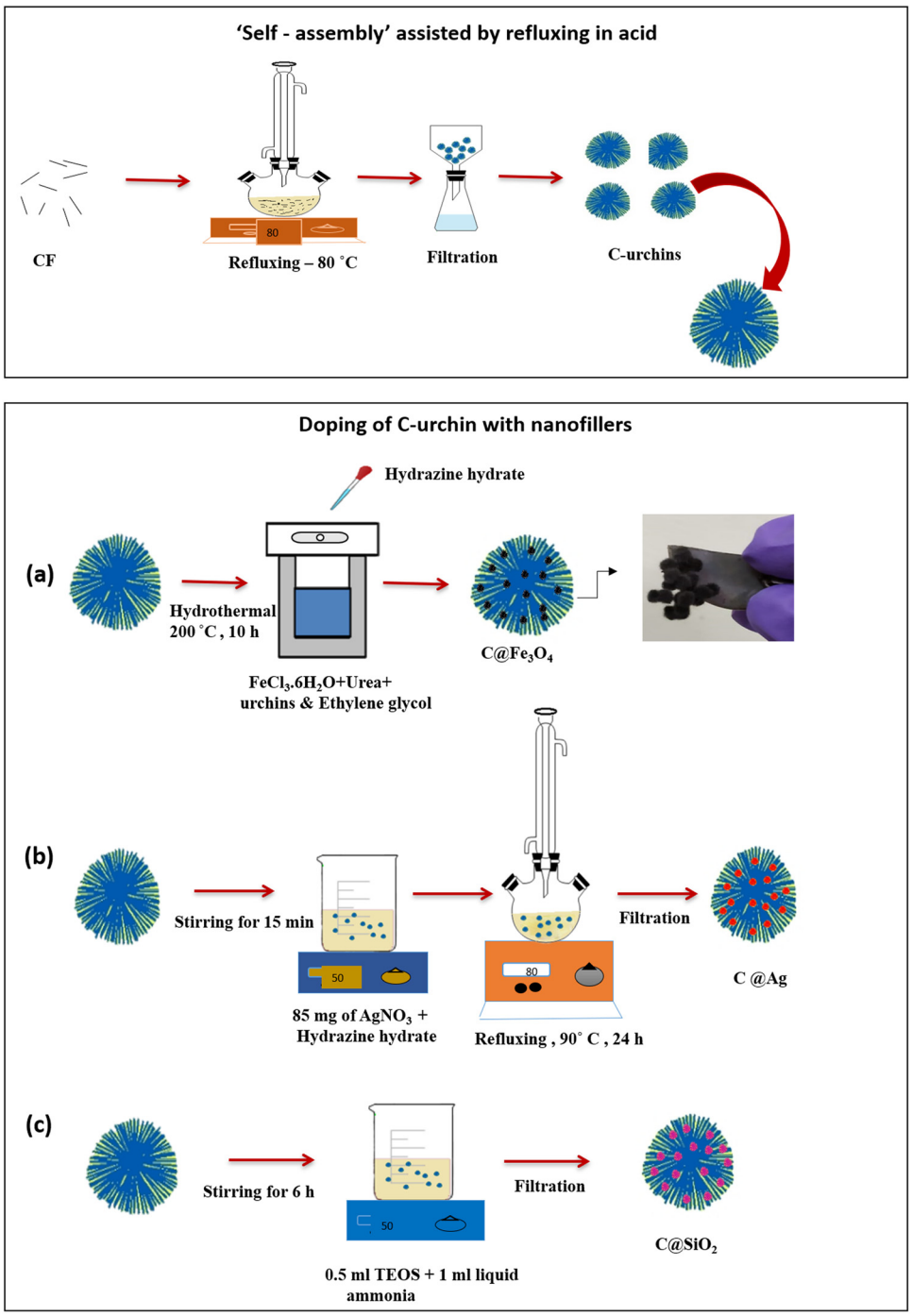

Fig. 1 A schematic diagram illustrating the synthesis of sea-urchin-like carbon structures derived from the 'self-assembly' of carbon fibers assisted by refluxing in an acid medium. The synthesis of (a) carbon urchins doped with Fe_3O_4 nanoparticles; (b) carbon urchins doped with Ag nanoparticles; and (c) carbon urchins doped with SiO_2 nanoparticles. The inset of (a) shows the magnetic nature of carbon urchins doped with Fe_3O_4 nanoparticles.

range (8.2 to 26.5 GHz) at room temperature. The scattering parameters (S_{11}, S_{12}, S_{21}, and S_{22}) obtained from VNA are used to evaluate the total shielding effectiveness (SE_T) and shielding effectiveness from absorption (SE_A) and reflection (SE_R). The magnetic properties were studied at room temperature (with an applied field of −40 000 to 40 000 Oe) using a vibrating sample magnetometer (VSM) bought from Lakeshore.

Results and discussion

Structural and spectroscopic analysis

The structures of C-urchins, C-F urchins, C-A urchins, and C-S urchins were assessed using XRD. The XRD patterns of the materials are shown in Fig. 3a. C-urchins showed a peak at around 25°, which corresponds to the (002) plane of carbon fibers.[43] In the XRD pattern of C-F urchins, five additional

Open Access Article. Published on 02 August 2022. Downloaded on 2/10/2026 5:06:23 AM.
This article is licensed under a Creative Commons Attribution-NonCommercial 3.0 Unported Licence.

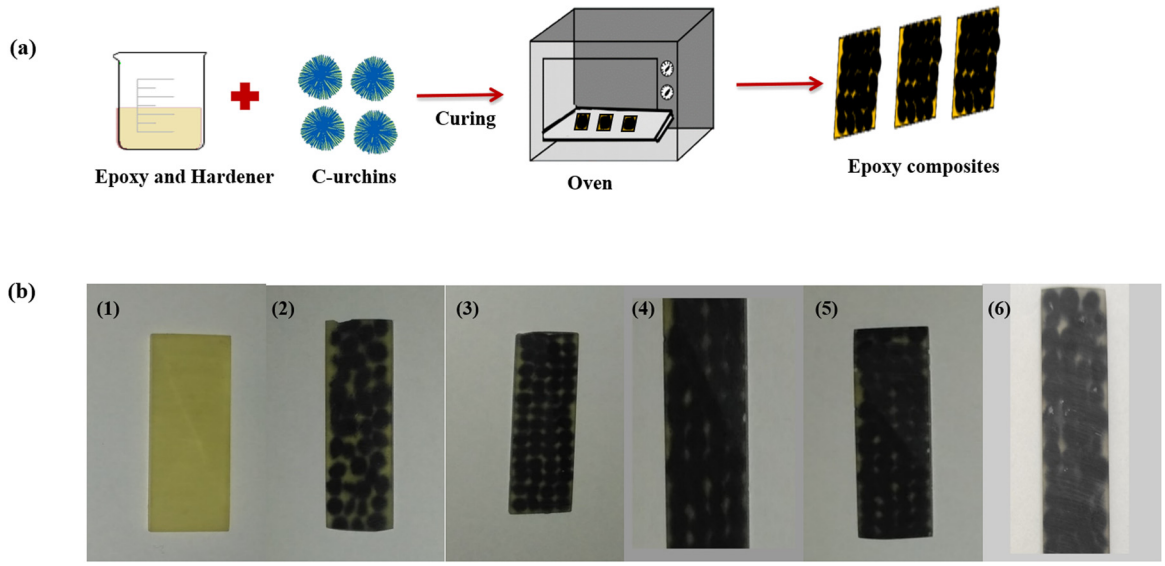

Fig. 2 (a) A schematic diagram illustrating the preparation of C-urchin/epoxy composites. (b) Digital photographs of the prepared composites: (1) neat epoxy, (2) C-urchins loosely packed, (3) C-urchins closely packed, (4) C-F urchins (closely packed), (5) C-A urchins (closely packed), and (6) C-S urchins (closely packed).

peaks were observed at 30.56°, 36.03°, 43.6°, 57.6°, and 63.3°, corresponding to the (220), (311), (400), (511), and (440) planes.[47] These peaks can be attributed to the formation of Fe_3O_4 nanoparticles on C-urchins after the hydrothermal reaction. Similarly, the XRD pattern of C-A urchins shows four peaks at 38.1°, 44.3°, 64.4°, and 77.4°, which correspond to the (111), (200), (220), and (311) diffraction planes, respectively, of face-centered cubic (fcc) Ag nanoparticles.[44] This is in accordance with the standard pattern (JCPDS card no 04-0783). For C-S urchins, the XRD pattern shows a characteristic amorphous hump at 23°, which can be attributed to SiO_2 nanoparticles.[48]

Fig. 3b shows the FTIR spectra of CF, C-urchins, C-F urchins, C-A urchins, and C-S urchins. The peak at 1704 cm^{-1} in the spectra of C-urchins and C-A urchins corresponds to C═O

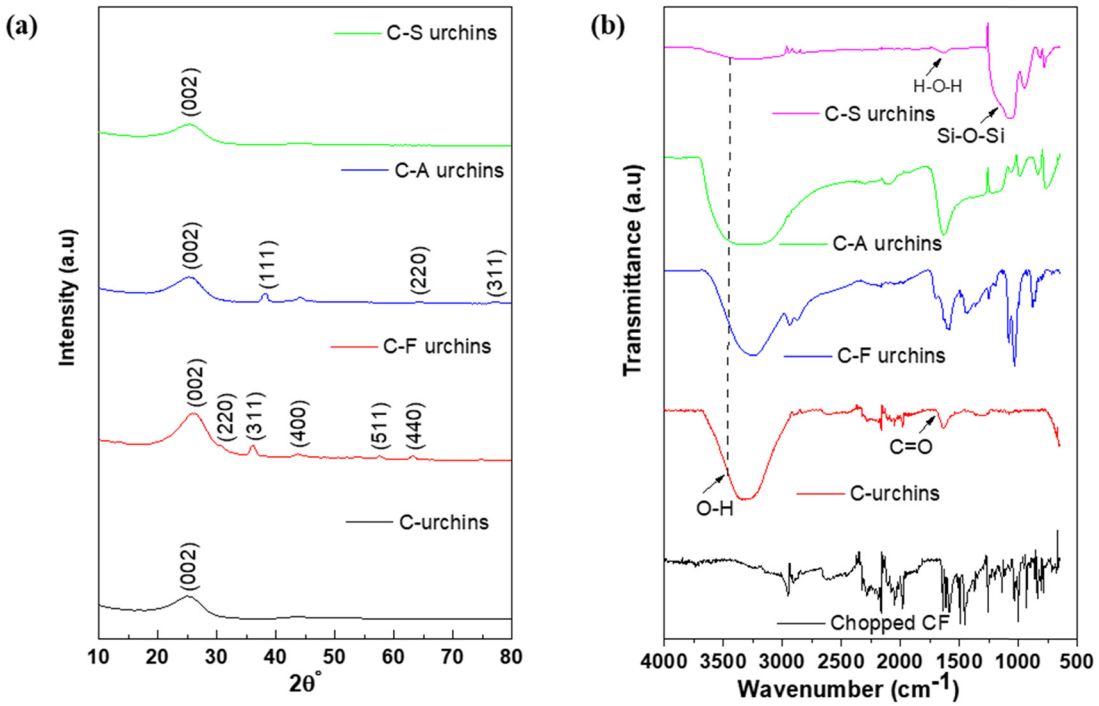

Fig. 3 (a) XRD patterns of C-urchins, C-F urchins, C-A urchins, and C-S urchins. (b) FT-IR spectra of CFs, C-urchins, C-F urchins, C-A urchins, and C-S urchins.

© 2022 The Author(s). Published by the Royal Society of Chemistry

Open Access Article. Published on 02 August 2022. Downloaded on 2/10/2026 5:06:23 AM.
This article is licensed under a Creative Commons Attribution-NonCommercial 3.0 Unported Licence.

carbonyl stretching. The reduced intensity of carbonyl stretching in the spectra of C-F urchins and C-S urchins suggests the utilization of carboxylic groups during the synthesis of doped C-urchins. A peak appears in all urchin spectra at around 3458 cm^{-1}, which corresponds to the stretching of hydrogen-bonded OH groups. The bands at around 1116 cm^{-1} and 1663 cm^{-1} in the spectra of C-S urchins correspond to H–O–H bending and Si–O–Si vibrations, respectively.[49]

Fig. 4(a) shows an SEM micrograph of CFs. Fig. 4(b and c) shows the 'self-assembled' micro-spikes resulting in a sea-urchin-like structure, and the higher magnification image of the urchins clearly shows that the microneedles could scatter/absorb radiation *via* coupling with incoming fields. Fig. 4(d–f) shows doped C-urchin with Fe_3O_4 (the presence of dopant can be clearly seen in high-magnification images). Fig. 4(g–i) depicts C-urchins doped with Ag, and Fig. 4(j–l) shows C-urchins doped with SiO_2 (the presence of dopants can be seen in higher-magnification images). From these micrographs, the presence of dopants on the C-urchins is clearly evident. Fig. 5(a–e) compares the surface morphologies of CFs, C-urchins, C-F urchins, C-A urchins, and C-S urchins, and EDS mapping analysis is provided. It is observed that the surface of C-urchins is smooth, whereas in the case of urchins anchoring Fe_3O_4, Ag, or SiO_2, white dots cover the surface of C-urchins, manifesting the presence of nanoparticles on the C-urchins after the reaction process. Estimates of the amounts of Fe_3O_4, Ag, and SiO_2 on the C urchin surfaces are determined *via* EDS analysis, which showed 8.38 atomic% for Fe, 4.60 atomic% for Ag, and 26.35 atomic% for Si.

Thermal and physical properties of the doped C-urchins. The thermal stability of the prepared composites was studied *via* TGA.[50] It is observed that the epoxy composites comprising C-F urchins were stable up to 350 °C, while C-A urchins and C-S urchins were stable up to 320 °C. The degradation plots for the

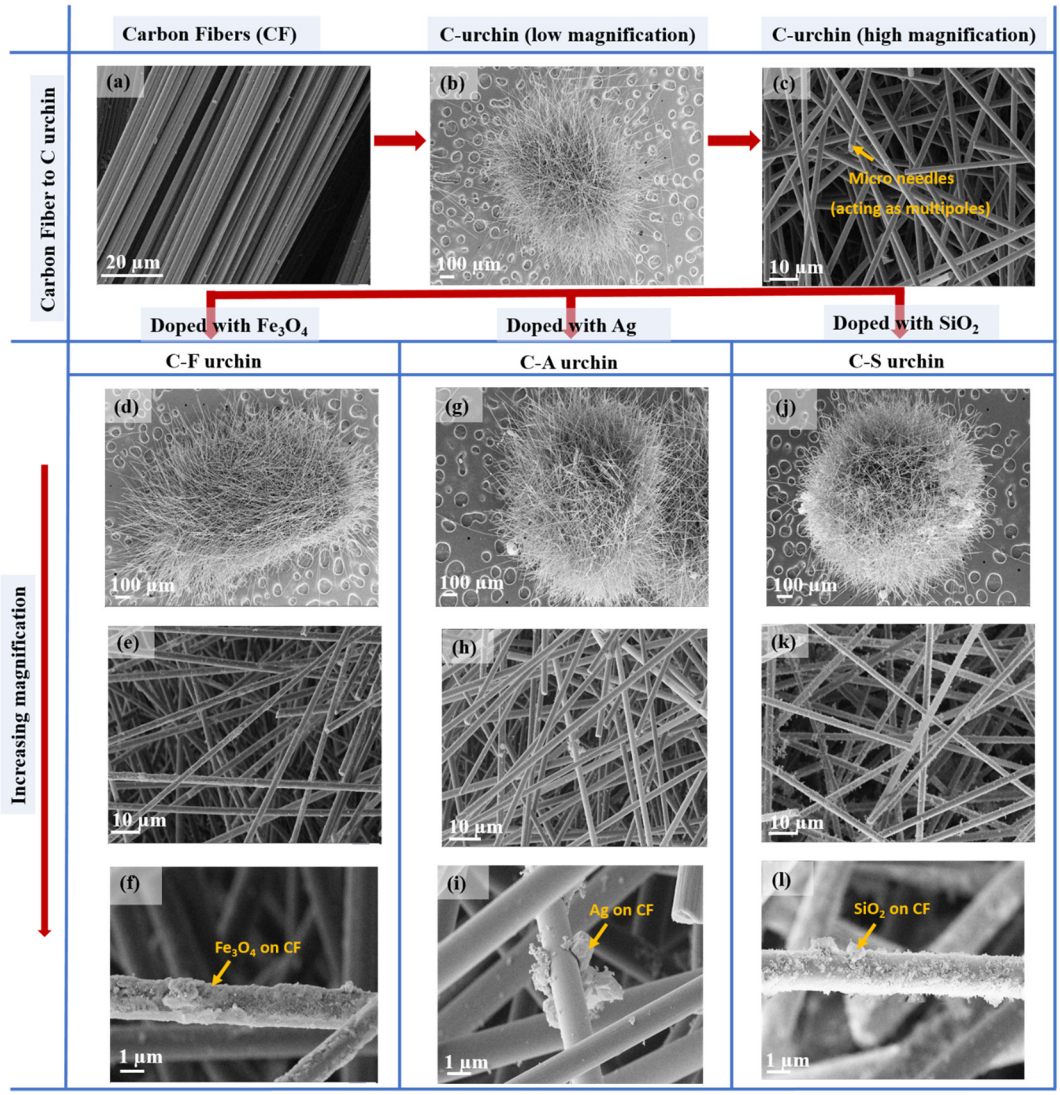

Fig. 4 SEM micrographs: (a) CFs; (b) C-urchins; (c) C-urchins (high magnification), depicting the presence of microneedles acting as multipoles; (d–f) C-urchins doped with Fe_3O_4 (arranged by increasing magnification from top to bottom); (g–i) C-urchins doped with Ag (arranged by increasing magnification from top to bottom); and (j–l) C-urchins doped with SiO_2 (arranged by increasing magnification from top to bottom).

Open Access Article. Published on 02 August 2022. Downloaded on 2/10/2026 5:06:23 AM.
This article is licensed under a Creative Commons Attribution-NonCommercial 3.0 Unported Licence.

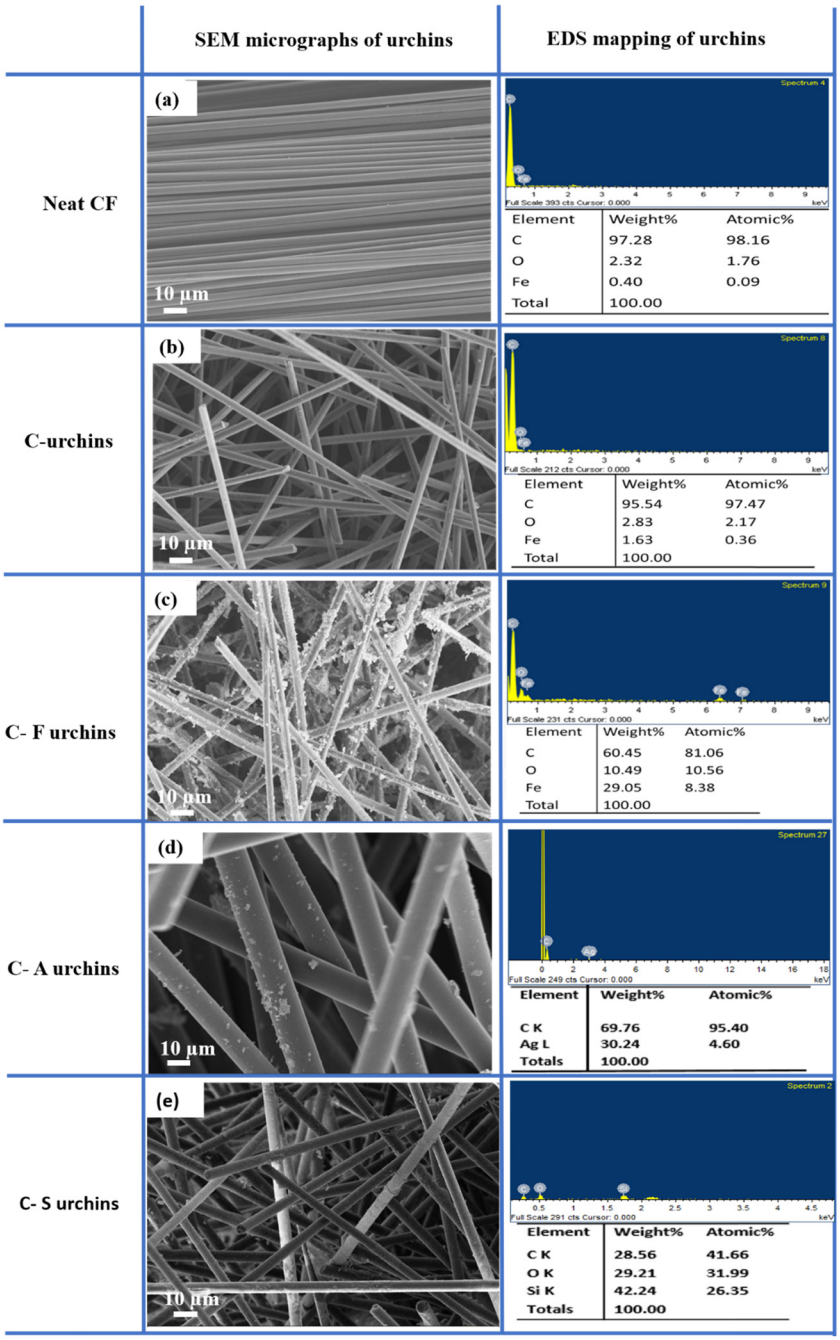

Fig. 5 SEM micrographs of (a) CFs, (b) C-urchins, (c) C-F urchins, (d) C-A urchins, and (e) C-S urchins with accompanying EDS elemental mapping analysis.

epoxy composites are shown in Fig. 6(a). It can be concluded that incorporating these carbon fillers had no detrimental effects on the thermal degradation properties of the composite system. To illustrate that the composite retained the magnetic properties of the C-F urchins, a bar magnet was used, and it can be clearly seen from the digital image in Fig. 6(b) that the composite with C-F urchins retained magnetic behavior.

The magnetic properties of C-F urchins and the epoxy composite containing C-F urchins were measured *via* VSM at room temperature. Fig. 6(c) shows the magnetic curves of C-F urchins and the C-F urchin composite. It can be observed that the saturation magnetization of the composites was reached rapidly. The saturation magnetization (H_s) and coercivity (H_c) of C-F urchins are 3.7 emu g^{-1} and 142.7 Oe, respectively, and those of the C-F urchin composite are 0.19 emu g^{-1} and 47.2 Oe, respectively. The H_s and H_c values of the C-F urchins are higher than the epoxy composite containing C-F urchins, which is as expected.

The mechanical properties of epoxy composites containing C-urchins and doped C-urchins were analyzed using DMA.

© 2022 The Author(s). Published by the Royal Society of Chemistry

Open Access Article. Published on 02 August 2022. Downloaded on 2/10/2026 5:06:23 AM.
This article is licensed under a Creative Commons Attribution-NonCommercial 3.0 Unported Licence.

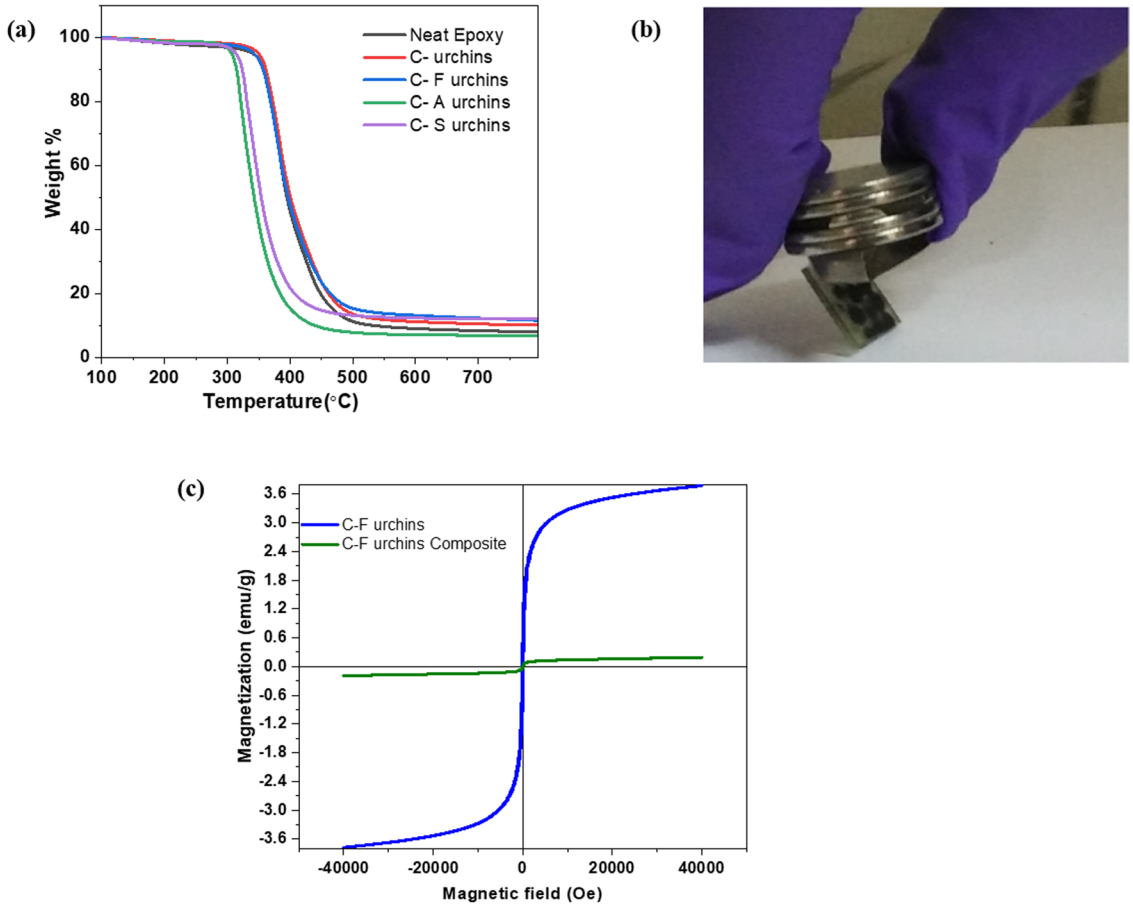

Fig. 6 (a) TGA analysis of the epoxy composites. (b) The magnetic properties of C-F urchins embedded in an epoxy matrix. (c) VSM plots for C-F urchins and the C-F-urchin-based composite.

Fig. 7 demonstrates the storage moduli and tan δ curves as a function of temperature for various epoxy composites. As seen in Fig. 7(a), it is observed that with the addition of C-urchins, C-F urchins, C-A urchins, and C-S urchins, the storage modulus reached 2117 MPa, 3074 MPa, 2858 MPa, and 2647 MPa, respectively, compared to neat epoxy, which showed a storage modulus of 2100 MPa. The enhancement in storage modulus in composites containing closely packed C-urchins is attributed to effective load transfer from epoxy to the filler material.[17,51] Fig. 7(b) shows the tan δ curves for the epoxy composites. T_g is around 135 °C for neat epoxy, whereas the T_g values for C-urchins, C-F urchins, C-A urchins, and C-S urchins were 137 °C, 142 °C, 142 °C, and 139 °C, respectively.

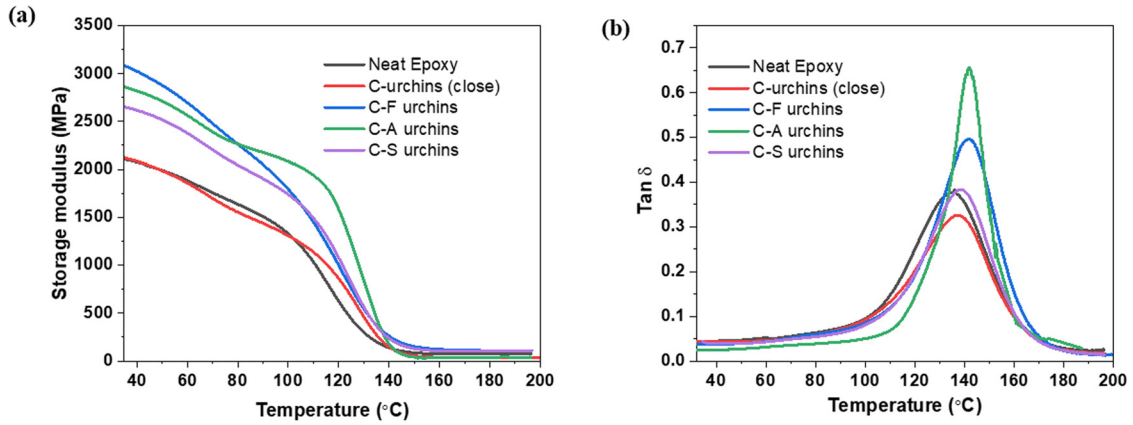

Fig. 7 (a) Storage modulus and (b) tan δ plots of epoxy composites obtained from DMA analysis.

Open Access Article. Published on 02 August 2022. Downloaded on 2/10/2026 5:06:23 AM. This article is licensed under a Creative Commons Attribution-NonCommercial 3.0 Unported Licence.

The flame retardancy of the epoxy composites was determined using LOI testing, which ultimately gives the flammability behavior of polymeric materials. The epoxy resin is highly flammable and showed an LOI value of 21. The epoxy composites containing C-urchins, C-F urchins, C-A urchins, and C-S urchins showed improvement in the LOI value to 22. This indicates that the addition of C-urchins can also improve the flammability properties to some extent compared to neat epoxy.[6]

AC electrical conductivity of composites. It is envisaged that electrical conductivity and interconnected networks of conducting nanofillers are essential factors that control the shielding mechanism. In general, a shielding material should have moderate to high electrical conductivity, as well as supporting magnetic and dielectric loss.[52] Fig. 8 shows the variation in the AC electrical conductivity with the frequency recorded at room temperature.

The Jonscher universal power law explains the frequency dependence of AC conductivity. According to the law, conducting filler in a polymer matrix can be modeled as a set of resistors and capacitors.[12] A plot shows that the AC electrical conductivity of the capacitor increases with frequency, and the resistor exhibits a frequency-independent response. The AC electrical conductivity as a function of frequency can be expressed *via* the following equation:

$$\sigma'(\omega) = \sigma(0) + \sigma_{AC}(\omega) = \sigma_{DC} + A\omega^{s} \quad (1)$$

where ω is the angular frequency, σ_{DC} is the direct electrical conductivity, A is a pre-exponential factor dependent on temperature, and s is an exponent.[53] Here, 's' represents the 3D network formed between the resistors and the capacitors, and it depends on temperature and frequency.[53] The value of 's' can range from 0–1. Hence, *via* fitting the power-law, the value of 's' can be calculated.

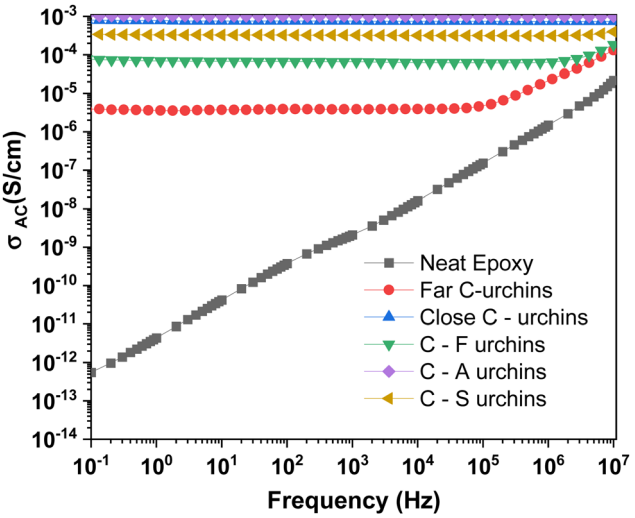

Fig. 8 AC electrical conductivity values of the composites as a function of frequency.

Since the host matrix (epoxy) is insulating in nature, the shielding efficiency depends on the network of conducting C-urchins or, more precisely, the spatial distribution of the urchins in the composite. From the data, the DC electrical conductivity values of the composites containing C-urchins that are closely packed, C-F urchins, C-A urchins, and C-S urchins are observed to be 7.04×10^{-4}, 8.55×10^{-5}, 1.06×10^{-3}, and 3.50×10^{-4} S cm^{-1}, respectively. Due to defects produced during harsh chemical refluxing (or during the hydrothermal reaction) in the case of doped C-urchins, we can conclude that the polarization centers thus generated can help in suppressing incoming EM radiation.

The closely packed urchins showed higher conductivity compared with other composites due to electron tunneling or hopping, as insulating epoxy at the interface offers contact resistance. Generally, these structures with closely packed C-urchins that showed higher electrical conductivity can be ideal candidates for shielding purposes.[54,55] To appreciate the efficacy of our strategy, we prepared a few composites with CNTs, varying their concentration in the epoxy matrix, and evaluated the shielding performance. The bulk electrical conductivity data for the composites with CNTs are shown in Fig. S1 (ESI†).

The values of 's' for closely packed C-urchins, C-A urchins, and C-S urchins begin to suggest that the composites are highly conducting over the entire measured frequency range. The values for C-urchins loosely packed and C-F urchins were less than 1. Hence, the charge transport phenomenon can either involve the tunneling or hopping of electrons.

EMI shielding effectiveness of the epoxy composites. The EMI shielding efficiency is expressed in terms of SE_T, which is a logarithmic quantity representing the ability of a material to shield against EM radiation.[4,56,57] The shielding efficiency (SE) is generally expressed in terms of the reduction in the magnitude of the incident power or field upon the transition across the shield, expressed in terms of electric field strength (E), magnetic field strength (H), or power (P). It can be referred to as the ratio of P(E or H) before attenuation to that of P(E or H) after attenuation, as shown in eqn (2):[7]

$$SE_T = -10 \log_{10} \frac{P_I}{P_T} \quad (2)$$

where P_I is the incident power and P_T is the transmitted power. SE_T is expressed in units of dB. For most commercial applications, the value of SE_T should be at least −20 dB, which indicates 99% attenuation of the waves.[58] There are three different main mechanisms that contribute to the SE_T value: shielding *via* reflection (SE_R), shielding *via* absorption (SE_A), and shielding *via* multiple reflection (SE_{MR}). SE_T is mathematically expressed as a summation of SE_R, SE_A, and SE_{MR}, as given below:[59]

$$SE_T = SE_A + SE_R + SE_{MR} \quad (3)$$

when the absorption of the penetrated waves increases and SE_T is more than −15 dB, SE_{MR} can be neglected, and eqn (3) can be re-written as:[7,60]

© 2022 The Author(s). Published by the Royal Society of Chemistry

Open Access Article. Published on 02 August 2022. Downloaded on 2/10/2026 5:06:23 AM.
This article is licensed under a Creative Commons Attribution-NonCommercial 3.0 Unported Licence.

$$SE \approx SE_R + SE_A \quad (4)$$

The SE values are practically determined from scattering parameters (*i.e.*, S_{11}, S_{22}, S_{12}, and S_{21}) obtained from the VNA data, as shown in eqn (5)–(7):

$$SE_T = 10 \log_{10} \frac{1}{|S_{21}|^2} = 10 \log_{10} \frac{1}{|S_{12}|^2} \quad (5)$$

$$SE_R = 10 \log_{10} \frac{1}{(1 - |S_{11}|^2)} \quad (6)$$

$$SE_A = \log_{10} \frac{1 - |S_{11}|_2}{|S_{21}|^2} = SE_T - SE_R \quad (7)$$

S_{11} and S_{22} are referred to as reflection coefficients and S_{21} and S_{12} are referred to as transmission coefficients.

Fig. 9(a) shows plots of SE_T for epoxy composites in the X (8.2–12.4 GHz), Ku (12.4–18 GHz), and K (18–26.5 GHz) band ranges. The SE_T value of a 1 mm-thick C-urchin/epoxy composite is found to be −24 dB. C-F, C-A, and C-S doped urchins showed SE_T values of −31 dB, −26 dB, and −32 dB, respectively, at 18 GHz. The amount of urchins in epoxy was estimated to be around 7 wt%. C-urchins that are loosely packed (control sample) resulted in an SE_T value of −21 dB for a 1 mm-thick composite. It is interesting to note that even when the urchins are loosely packed, the bulk electrical conductivity is as high as 3×10^{-6} S cm^{-1}, which begins to suggest that electron transport is facilitated through hopping. When the urchins are closely packed (touching each other), the interconnected pathways due to the conducting filler lead to higher conductivity and SE_T values. To further understand the shielding mechanism, $\%SE_A$ and $\%SE_R$ values were evaluated and plotted against frequency, as shown in Fig. 9(b). From Fig. 9(b), it is observed that the shielding mechanism is absorption-dominated, which can be attributed to conduction loss (due to the interconnected urchin network), dielectric loss (depending on the filler and interfaces), and also multiple internal reflection (at urchin-polymer and urchin-particle interfaces). The magnetic, conducting, or dielectric nanostructures anchored onto the urchins interact with the incoming EM field and contribute to the loss, which results in slightly higher absorption percentages compared to the neat C-urchin-based composite.[45,61,62] For comparison purposes, the SE_T values of 0.5 wt% CNTs and 1 wt% CNTs were also measured (refer to Fig. S2, ESI†).

Heat dissipation testing was performed, and a heat mapping plot is shown in Fig. 9(c). The mapping was done for the EMI shield which exhibited the highest SE_T value. In the heat dissipation test, a laser beam was used to heat the sample for 50 s and the temperature was measured as a function of time. Then the laser was switched off and the shield was allowed to cool down for 50 s. The temperature dropped from 126.5 °C to room temperature within 60 s, suggesting quick heat dissipation within the EMI shield.

A schematic diagram illustrating the mechanism of shielding is given in Fig. 10. The micro-spikes on the C-urchins can

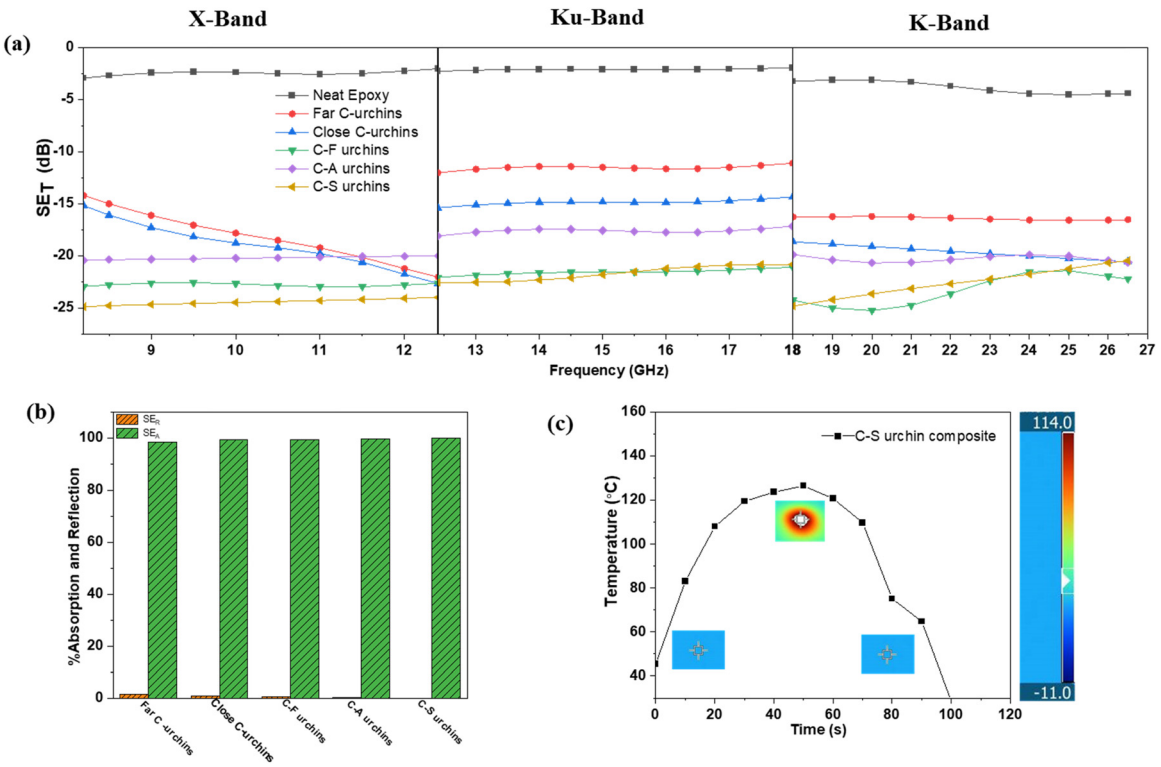

Fig. 9 (a) Plots of SE_T vs frequency for the epoxy composites in different band regions. (b) %Absorption and reflection in epoxy composites at 26.5 GHz. (c) A heat dissipation plot for the C-S urchin composite.

Open Access Article. Published on 02 August 2022. Downloaded on 2/10/2026 5:06:23 AM.
This article is licensed under a Creative Commons Attribution-NonCommercial 3.0 Unported Licence.

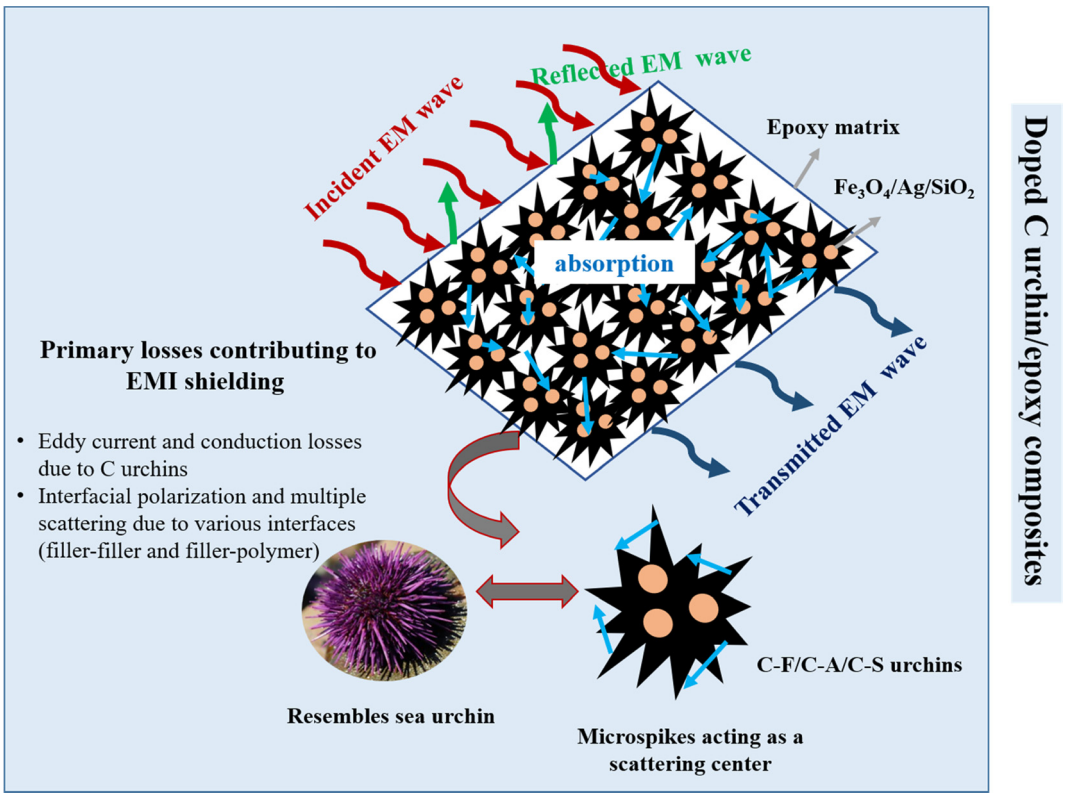

Fig. 10 The mechanism of shielding for doped-C-urchin/epoxy-based composites.

effectively scatter/absorb incoming EM waves. For each C-urchin, the assembly of spikes obtained during synthesis with different densities can result in varying degrees of absorption. This will also depend on the spatial distribution of C-urchins in the composite. Moreover, the large aspect ratio of the micro-spikes can result in a concentrated magnetic field at the tip under irradiating EM waves with an alternating polarization vector direction. Thus the concentrated tips will act as multi-poles, resulting in strong absorption due to coupling with the incident magnetic field, very similar to lightning rods.[63,64] Taken together, our study begins to suggest that this self-assembly of micro-spikes (during synthesis), resulting in a sea-urchin-like structure, can facilitate more absorption than conventional dispersed-flake composites. Moreover, the ease of dispersion and the control of the spatial distribution of urchins make this approach quite attractive in terms of processing.

Conclusions

In summary, a facile strategy for fabricating 'sea-urchin'-like carbon structures self-assembled from short carbon fibers is demonstrated here. When their spatial distribution is well controlled, the composites with epoxy suppressed EM radiation to a great extent. Furthermore, magnetic (Fe_3O_4), conducting (Ag), and dielectric (SiO_2) nanoparticles were doped in turn onto the C-urchins to enhance the absorption-based shielding. Epoxy composites with C, C-F, C-A, and C-S urchins were prepared following pre- and post-curing cycles. The spatial distribution of the urchins was controlled to gain mechanistic insight into the shielding efficiency. The remarkable improvement in electrical conductivity (7.04×10^{-4} S cm^{-1}) in the case of the composite containing closely packed C-urchins begins to suggest the presence of an interconnected conducting network that can add to the conduction and eddy current loss. All the doped C-urchins exhibited shielding effectiveness between −26 dB and −32 dB for 1 mm-thick samples in the K band; while these values are higher than the control sample, the nature of the dopant did not alter the shielding effectiveness to a large extent. In addition, absorption-dominated shielding was also seen for all doped C-urchins. Apart from improved shielding performance, the composites exhibited enhanced storage modulus values coupled with high thermal stability. In addition, the LOI values suggest that the flame-retardant properties are also slightly enhanced, manifesting that these samples can further be explored for aerospace applications. Taken together, our results offer a simple strategy for synthesizing sea-urchin-like carbon structures *via* the facile self-assembly of carbon fibers following refluxing in an acid medium. Also, these C-urchins are easy to disperse at length scales that are not available with conventional dispersed-flake composites.

Conflicts of interest

There are no conflicts to declare.

© 2022 The Author(s). Published by the Royal Society of Chemistry

Open Access Article. Published on 02 August 2022. Downloaded on 2/10/2026 5:06:23 AM. This article is licensed under a Creative Commons Attribution-NonCommercial 3.0 Unported Licence.

Acknowledgements

The authors would like to acknowledge financial support from DST, India, and IISc for various characterization facilities. The authors would also like to thank Jagadeshvaran PL, Devansh Sharma and Sankeerthana Avasarala for their help with performing certain characterization studies.

References

1 M. K. Vyas and A. Chandra, Ion–electron-conducting polymer composites: promising electromagnetic interference shielding material, *ACS Appl. Mater. Interfaces*, 2016, **8**(28), 18450–18461.
2 Y.-D. Shi, J. Li, Y.-J. Tan, Y.-F. Chen and M. Wang, Percolation behavior of electromagnetic interference shielding in polymer/multi-walled carbon nanotube nanocomposites, *Compos. Sci. Technol.*, 2019, **170**, 70–76.
3 S. Sankaran, K. Deshmukh, M. B. Ahamed and S. K. Pasha, Recent advances in electromagnetic interference shielding properties of metal and carbon filler reinforced flexible polymer composites: a review, *Composites, Part A*, 2018, **114**, 49–71.
4 A. Joshi and S. Datar, Carbon nanostructure composite for electromagnetic interference shielding, *Pramana*, 2015, **84**(6), 1099–1116.
5 C. Wang, V. Murugadoss, J. Kong, Z. He, X. Mai, Q. Shao, Y. Chen, L. Guo, C. Liu and S. Angaiah, Overview of carbon nanostructures and nanocomposites for electromagnetic wave shielding, *Carbon*, 2018, **140**, 696–733.
6 S. Mishra, P. Katti, S. Kumar and S. Bose, Macroporous epoxy-carbon fiber structures with a sacrificial 3D printed polymeric mesh suppresses electromagnetic radiation, *Chem. Eng. J.*, 2019, **357**, 384–394.
7 K. Sushmita, G. Madras and S. Bose, The journey of polycarbonate-based composites towards suppressing electromagnetic radiation, *Funct. Compos. Mater.*, 2021, **2**(1), 13.
8 K. Sushmita, G. Madras and S. Bose, Polymer Nanocomposites Containing Semiconductors as Advanced Materials for EMI Shielding, *ACS Omega*, 2020, **5**(10), 4705–4718.
9 S. P. Pawar, P. Rzeczkowski, P. Pötschke, B. Krause and S. Bose, Does the Processing Method Resulting in Different States of an Interconnected Network of Multiwalled Carbon Nanotubes in Polymeric Blend Nanocomposites Affect EMI Shielding Properties?, *ACS Omega*, 2018, **3**(5), 5771–5782.
10 K. Sushmita, S. Maiti and S. Bose, Multi-layered composites using polyurethane-based foams and 3D-printed structures to curb electromagnetic pollution, *Mater. Adv.*, 2022, **3**, 4578–4599.
11 S. Sankaran, K. Deshmukh, M. B. Ahamed and S. K. Khadheer Pasha, Recent advances in electromagnetic interference shielding properties of metal and carbon filler reinforced flexible polymer composites: A review, *Composites, Part A*, 2018, **114**, 49–71.
12 K. Sushmita, A. V. Menon, S. Sharma, A. C. Abhyankar, G. Madras and S. Bose, Mechanistic insight into the nature of dopant in graphene derivative influencing EMI shielding properties in hybrid polymer nanocomposites, *J. Phys. Chem. C*, 2019, **123**(4), 2579–2590.
13 P. K. Balguri, D. G. H. Samuel and U. Thumu, A review on mechanical properties of epoxy nanocomposites, *Mater. Today: Proc.*, 2021, **44**, 346–355.
14 F.-L. Jin, X. Li and S.-J. Park, Synthesis and application of epoxy resins: A review, *J. Ind. Eng. Chem.*, 2015, **29**, 1–11.
15 M. A. Boyle, C. J. Martin and J. D. Neuner, Epoxy resins, *ASM handbook*, 2001, **21**, 78–89.
16 J.-P. Pascault; H. Sautereau; J. Verdu and R. J. Williams, *Thermosetting polymers*. Marcel Dekker New York, 2002, vol. 477.
17 P. Katti, S. Bose and S. Kumar, Tailored interface resulting in improvement in mechanical properties of epoxy composites containing poly (ether ether ketone) grafted multiwall carbon nanotubes, *Polymer*, 2016, **102**, 43–53.
18 A. Vincent, G. Ramesh and S. M. Kumar, Microwave Shielding Behaviour of Surface Treated MWCNT-epoxy Composites in I & J Band-A Note, *Colloid Interface Sci. Commun.*, 2018, **24**, 89–92.
19 J. Wu and D. Chung, Increasing the electromagnetic interference shielding effectiveness of carbon fiber polymer–matrix composite by using activated carbon fibers, *Carbon*, 2002, **40**(3), 445–447.
20 K. Sushmita; G. Madras and S. J. F. C. M. Bose, The journey of polycarbonate-based composites towards suppressing electromagnetic radiation, 2021, **2**(1), 1–38.
21 R. Rohini; K. Verma and S. J. A. O. Bose, Interfacial architecture constructed using functionalized MWNT resulting in enhanced EMI shielding in epoxy/carbon fiber composites, 2018, **3**(4), 3974–3982.
22 Y. Bhattacharjee, D. Chatterjee and S. Bose, Core–Multishell Heterostructure with Excellent Heat Dissipation for Electromagnetic Interference Shielding, *ACS Appl. Mater. Interfaces*, 2018, **10**(36), 30762–30773.
23 C. Liang, Z. Gu, Y. Zhang, Z. Ma, H. Qiu and J. Gu, Structural Design Strategies of Polymer Matrix Composites for Electromagnetic Interference Shielding: A Review, *Nano-Micro Lett.*, 2021, **13**(1), 181.
24 N. Bagotia, V. Choudhary and D. K. Sharma, A review on the mechanical, electrical and EMI shielding properties of carbon nanotubes and graphene reinforced polycarbonate nanocomposites, *Polym. Adv. Technol.*, 2018, **29**(6), 1547–1567.
25 G. Mittal, V. Dhand, K. Y. Rhee, S.-J. Park and W. R. Lee, A review on carbon nanotubes and graphene as fillers in reinforced polymer nanocomposites, *J. Ind. Eng. Chem.*, 2015, **21**, 11–25.
26 D. Wanasinghe, F. Aslani, G. Ma and D. Habibi, Review of polymer composites with diverse nanofillers for electromagnetic interference shielding, *Nanomaterials*, 2020, **10**(3), 541.
27 K. Rengaswamy; D. K. Sakthivel; A. Muthukaruppan; B. Natesan; S. Venkatachalam and D. J. N. J. O. C. Kannaiyan, Electromagnetic interference (EMI) shielding performance of

Open Access Article. Published on 02 August 2022. Downloaded on 2/10/2026 5:06:23 AM. This article is licensed under a Creative Commons Attribution-NonCommercial 3.0 Unported Licence.

lightweight metal decorated carbon nanostructures dispersed in flexible polyvinylidene fluoride films, 2018, **42**(15), 12945–12953.

28 A. A. Eddib and D. Chung, Electric permittivity of carbon fiber, *Carbon*, 2019, **143**, 475–480.

29 T. K. Das, P. Ghosh and N. C. Das, Preparation, development, outcomes, and application versatility of carbon fiber-based polymer composites: a review, *Adv. Compos. Hybrid Mater.*, 2019, 1–20.

30 T. Xiao, J. Kuang, P. Sun, X. Hou, Q. Wang, P. Jiang and W. Cao, Rapid microwave synthesis of coaxial SiC/carbon fibre (SiC/CF) with improved oxidation resistance and wettability, *Ceram. Int.*, 2019, **45**(2), 2432–2438.

31 S. Chand, Review carbon fibers for composites, *J. Mater. Sci.*, 2000, **35**(6), 1303–1313.

32 T. Gayathri, N. Kavitha, A. Chandramohan, D. Roy and K. J. M. T. P. Dinakaran, Mesoporous zirconia nanostructures embedded Polyvinyledine difluoride conducting films for EMI shielding applications, 2022, **59**, 534–539.

33 K. Dinakaran, K. Narayanasamy, S. Theerthagiri, P. Peethambaram, S. Krishnan and D. J. I. J. O. P. A. Roy, Characterization, Microwave absorption and dielectric behavior of lead sulfide–graphene composite nanostructure embedded polyvinylidinedilfuoride thin films, 2022, 1–12.

34 K. Rengaswamy; V. K. Asapu; A. Muthukaruppan; D. K. Sakthivel; S. Venkatachalam and D. J. P. F. A. T. Kannaiyan, Enhanced shielding of electromagnetic radiations with flexible, light-weight, and conductive Ag-Cu/MWCNT/rGO architected PVDF nanocomposite films. 2021, 32 (9), 3759–3769.

35 M. Gholampoor; F. Movassagh-Alanagh and H. J. S. S. S. Salimkhani, Fabrication of nano-Fe3O4 3D structure on carbon fibers as a microwave absorber and EMI shielding composite by modified EPD method. 2017, 64, 51–61.

36 B. Cheng, J. Wang, F. Zhang and S. J. P. B. Qi, *Preparation of silver/carbon fiber/polyaniline microwave absorption composite and its application in epoxy resin*, 2018, **75**(1), 381–393.

37 F. Movassagh-Alanagh, S. Jalilian, R. Shemshadi and A. J. S. M. Kavianpour, *Fabrication of microwave absorbing Fe3O4/MWCNTs@ CFs nanocomposite by means of an electrophoretic co-deposition process*, 2019, **250**, 20–30.

38 Y. Wei, J. Yue, X.-Z. Tang, Z. Du and X. Huang, Enhanced magnetic and microwave absorption properties of FeCo-SiO2 nanogranular film functionalized carbon fibers fabricated with the radio frequency magnetron method, *Appl. Surf. Sci.*, 2018, **428**, 296–303.

39 B. Zhao, G. Shao, B. Fan, W. Zhao and R. Zhang, Investigation of the Electromagnetic Absorption Properties of Ni@TiO2 and Ni@SiO2 Composite Microspheres with Core-Shell Structure, *Phys. Chem. Chem. Phys.*, 2015, **17**, 2531.

40 Y. Ren, C. Zhu, S. Zhang, C. Li, Y. Chen, P. Gao, P. Yang and Q. Ouyang, Three-Dimensional SiO2@Fe3O4 Core/Shell Nanorod Array/Graphene Architecture: Synthesis and Electromagnetic Absorption Properties, *Nanoscale*, 2013, **5**, 12296.

41 F. Movassagh-Alanagh, A. Bordbar-Khiabani and A. Ahangari-Asl, Three-phase PANI@ nano-Fe3O4@ CFs heterostructure: Fabrication, characterization and investigation of microwave absorption and EMI shielding of PANI@ nano-Fe3O4@ CFs/epoxy hybrid composite, *Compos. Sci. Technol.*, 2017, **150**, 65–78.

42 Y. Liu, Z. Chen, W. Xie, S. Song, Y. Zhang and L. Dong, In-situ Growth and Graphitization Synthesis of Porous Fe3O4/Carbon Fiber Composites Derived from Biomass as Lightweight Microwave Absorber, *ACS Sustainable Chem. Eng.*, 2019, **7**(5), 5318–5328.

43 A. V. Menon, G. Madras and S. Bose, Ultrafast Self-Healable Interfaces in Polyurethane Nanocomposites Designed Using Diels–Alder ''Click'' as an Efficient Microwave Absorber, *ACS Omega*, 2018, **3**(1), 1137–1146.

44 S. P. Pawar, S. Kumar, S. Jain, M. Gandi, K. Chatterjee and S. J. N. Bose, Synergistic interactions between silver decorated graphene and carbon nanotubes yield flexible composites to attenuate electromagnetic radiation, 2016, **28**(2), 025201.

45 Y. Bhattacharjee, D. Chatterjee and S. J. A. A. M. Bose, Interfaces, Core–multishell heterostructure with excellent heat dissipation for electromagnetic interference shielding, 2018, **10**(36), 30762–30773.

46 R. Rohini and S. Bose, Tailored interface and enhanced elastic modulus in epoxy-based composites in presence of branched poly (ethyleneimine) grafted multiwall carbon nanotubes, *Phys. Chem. Chem. Phys.*, 2015, **17**(12), 7907–7913.

47 P. K. Samantaray, S. Baloda, G. Madras and S. Bose, Interlocked Dithi-Magnetospheres–Decorated MoS2 Nanosheets as Molecular Sieves and Traps for Heavy Metal Ions, *Adv. Sustainable Syst.*, 2019, 1800153.

48 A. Shalaby, V. Yaneva, A. Staneva, L. Aleksandrov, R. Iordanova and Y. J. N. N. Dimitriev, Thermal stability of RGO and RGO/SiO_2 nanocomposite prepared by sol-gel technique, 2014, **14**, 120.

49 T. Zhang, Y. Song, Y. Zhao, B. J. C. Zhang, S. A. Physicochemical and E. Aspects, *Effect of hybrid sizing with nano-SiO2 on the interfacial adhesion of carbon fibers/nylon 6 composites*, 2018, **553**, 125–133.

50 A. Chaudhary, R. Kumar, S. Teotia, S. Dhawan, S. R. Dhakate and S. Kumari, Integration of MCMBs/MWCNTs with Fe 3 O 4 in a flexible and light weight composite paper for promising EMI shielding applications, *J. Mater. Chem. C*, 2017, **5**(2), 322–332.

51 P. Katti, K. Kundan, S. Kumar and S. Bose, Poly (ether ether ketone)-Grafted Graphene Oxide ''Interconnects'' Enhance Mechanical, Dynamic Mechanical, and Flame-Retardant Properties in Epoxy Laminates, *ACS Omega*, 2018, **3**(12), 17487–17495.

52 S. P. Pawar, S. Biswas, G. P. Kar and S. Bose, High frequency millimetre wave absorbers derived from polymeric nanocomposites, *Polymer*, 2016, **84**, 398–419.

53 H. Nallabothula, Y. Bhattacharjee, L. Samantara and S. Bose, Processing-Mediated Different States of Dispersion of Multiwalled Carbon Nanotubes in PDMS Nanocomposites Influence EMI Shielding Performance, *ACS Omega*, 2019, **4**(1), 1781–1790.

 © 2022 The Author(s). Published by the Royal Society of Chemistry

Open Access Article. Published on 02 August 2022. Downloaded on 2/10/2026 5:06:23 AM.
This article is licensed under a Creative Commons Attribution-NonCommercial 3.0 Unported Licence.

54 R. Chippendale and I. O. Golosnoy, In Percolation effects in electrical conductivity of carbon fibre composites, IET 8th International Conference on Computation in Electromagnetics (CEM 2011), IET, 2011, pp. 1–2.
55 Y. Xi, Y. Bin, C. Chiang and M. Matsuo, Dielectric effects on positive temperature coefficient composites of polyethylene and short carbon fibers, *Carbon*, 2007, **45**(6), 1302–1309.
56 M. H. Al-Saleh and U. Sundararaj, Electromagnetic interference shielding mechanisms of CNT/polymer composites, *Carbon*, 2009, **47**(7), 1738–1746.
57 H. Hekmatara, M. Seifi, K. Forooraghi and S. J. P. C. C. P. Mirzaee, *Synthesis and microwave absorption characterization of SiO 2 coated Fe 3 O 4–MWCNT composites*, 2014, **16**(43), 24069–24075.
58 N. Li, Y. Huang, F. Du, X. He, X. Lin, H. Gao, Y. Ma, F. Li, Y. Chen and P. C. Eklund, Electromagnetic interference (EMI) shielding of single-walled carbon nanotube epoxy composites, *Nano Lett.*, 2006, **6**(6), 1141–1145.
59 A. D. S. Gomes, New polymers for special applications. BoD–Books on Demand, 2012.
60 P. Saini, V. Choudhary, B. Singh, R. Mathur and S. Dhawan, Polyaniline–MWCNT nanocomposites for microwave absorption and EMI shielding, *Mater. Chem. Phys.*, 2009, **113**(2-3), 919–926.
61 A. V. Menon, G. Madras and S. Bose, Phase specific dispersion of functional nanoparticles in soft nanocomposites resulting in enhanced electromagnetic screening ability dominated by absorption, *Phys. Chem. Chem. Phys.*, 2017, **19**(1), 467–479.
62 A. V. Menon, G. Madras and S. Bose, Magnetic Alloy-MWNT Heterostructure as Efficient Electromagnetic Wave Suppressors in Soft Nanocomposites, *ChemistrySelect*, 2017, **2**(26), 7831–7844.
63 C. Wang, X. Han, X. Zhang, S. Hu, T. Zhang, J. Wang, Y. Du, X. Wang and P. J. T. J. O. P. C. C. Xu, *Controlled synthesis and morphology-dependent electromagnetic properties of hierarchical cobalt assemblies*, 2010, **114**(35), 14826–14830.
64 C. Wang, X. Han, P. Xu, J. Wang, Y. Du, X. Wang, W. Qin and T. J. T. J. O. P. C. C. Zhang, Controlled synthesis of hierarchical nickel and morphology-dependent electromagnetic properties, 2010, **114**(7), 3196–3203.